Synthesis and Characterization of Star-Shaped Poly(*N*,*N*-dimethylaminoethyl methacrylate) and Its Quaternized Ammonium Salts

Felix A. Plamper,[†] Alexander Schmalz,[†] Evis Penott-Chang,[†] Markus Drechsler,[†] Arben Jusufi,[‡] Matthias Ballauff,[‡] and Axel H. E. Müller*,[†]

Makromolekulare Chemie II, Physikalische Chemie I, and Bayreuther Zentrum für Kolloide und Grenzflächen, Universität Bayreuth, D-95440 Bayreuth, Germany

Received February 21, 2007; Revised Manuscript Received May 29, 2007

ABSTRACT: We report on the synthesis and characterization of star-shaped strong polyelectrolytes and their precursor stars with up to 24 arms. To achieve this we polymerized 2-(*N*,*N*-dimethylamino)ethyl methacrylate (DMAEMA) by atom transfer radical polymerization employing a core-first attempt. Sugar-based scaffolds as well as silsesquioxane nanoparticles were used as oligofunctional initiators. Subsequent quaternization of the obtained poly(DMAEMA) stars yielded star-shaped poly{[2-(methacryloyloxy)ethyl] trimethylammonium iodide} (PMETAI). The initiation site efficiency was determined both by molecular weight measurements of the cleaved arms and by a statistical method after partial destruction of the inorganic core. The rather low efficiency of the initiation sites (30−75%) leads to a moderate arm number distribution of the prepared polyelectrolyte stars. As expected, the hydrodynamic radii of these polyelectrolyte stars decrease with increasing ionic strength. However, if the ionic strength was adjusted with NaI instead of NaCl, pronounced ion-specific effects were observed; the star polyelectrolyte first strongly shrinks with increasing salt concentration and becomes insoluble at about 0.5 M NaI ("salting out"). Still higher concentrations of NaI lead to a redissolution and a reswelling of the star polyelectrolyte ("salting in"). The measured osmotic coefficients are low and decrease with increasing arm number from $\phi \sim 0.12$ for a 3-arm star down to $\phi \sim 0.04$ for an 18-arm star, confirming the expected strong counterion confinement within these objects with high charge density.

Introduction

Polymers, in particular polyelectrolytes, with nonlinear topologies behave differently in many aspects compared to their linear counterparts. For example the counterions of a star-shaped polyelectrolyte and of densely grafted polyelectrolyte brushes are strongly confined within the macroion as opposed to linear architecture.[1−3] Hence the osmotic coefficient, ϕ, which is defined as the ratio of measured osmotic pressure to the ideal one is therefore lower than for linear polyelectrolytes.[2] Recent work on the osmotic coefficient of spherical polyelectrolyte brushes[4] demonstrated that ϕ measured in strictly salt-free systems is only of the order of a few percent and hence much lower than the value of 0.2−0.3 found for highly charged linear chains.[5] This is in full accord with recent theoretical deductions,[6] which suggest that the confinement of counterions should increase with increasing mutual interaction of the polyelectrolyte chains. In the case of polyelectrolyte stars this reasoning leads to the prediction that the osmotic coefficient should decrease with increasing arm number.[3]

While the confinement of counterions within spherical polyelectrolyte brushes seems to be a well-studied problem by now, information on polyelectrolyte stars is scarce. Recently, we showed that star-shaped poly(acrylic acid) with a rather low degree of neutralization exhibits indeed the expected decrease of the osmotic coefficient with increasing arm number.[7] However, the degree of neutralization of these *annealed* (weak) star polyelectrolytes was low ($\alpha \sim 0.25$) and reliable data suitable for a comparison with theory[3] could only be obtained for higher arm numbers. Here we wish to pursue this work by studying a *quenched* polyelectrolyte star, that is, a star polymer set up by strong polyelectrolyte chains whose charge density along the backbone is independent of the pH. This also alleviates the necessity to adjust a rather high pH value for a high degree of neutralization which may degrade the cores of the star polymers through hydrolysis.

The first syntheses leading to cationic/protonizable star-shaped polyelectrolytes were achieved by polymerization of vinylpyridine.[8,9] Heteroarm stars with long poly(2-vinylpyridine) (P2VP) and short polystyrene arms were made by microgel formation of short polystyrene chains with a difunctional monomer and polymerization of P2VP from the microgel bearing a large number of active sites.[10] A similar route was taken for the preparation of poly(*N*,*N*-dimethylaminoethyl methacrylate) (PDMAEMA) stars by group transfer polymerization.[11−13] These arm-first methods with difunctional monomers led to fairly large arm numbers, albeit with broad arm number distributions (e.g., $PDI_{app} > 1.6$).[12] In addition, a fraction of linear precursor polymer remains unreacted and therefore is not incorporated in the star.[11] The core-first method circumvents this problem when a defined initiator with a high initiation site efficiency is used. Cyclodextrin- and other sugar-based initiators are widely used scaffolds for this purpose and were also used by us for the synthesis of star-shaped poly(acrylic acid) by atom transfer radical polymerization (ATRP).[7,14,15] ATRP with multifunctional initiator also has been used for the synthesis of both weak and strong cationic polyelectrolyte stars. Partially functionalized β-cyclodextrin was used to form the core of PDMAEMA arms (arm number up to 4.5).[16] The use of quaternized DMAEMA as monomer in aqueous solution directly yields strong poly-

* Corresponding author. E-mail: axel.mueller@uni-bayreuth.de. Fax: +49-921-553393.
[†] Makromolekulare Chemie II, Universität Bayreuth.
[‡] Physikalische Chemie I, Universität Bayreuth.

10.1021/ma070452x CCC: $37.00
Published on Web 07/06/2007

electrolytes. However the limited solubility of a fully functionalized β-cyclodextrin initiator in water led to rather broad molecular weight distributions and fairly unsatisfactory control of the molecular weights (molecular weights were up to two times higher than expected).[17]

In this paper we report the synthesis of well-defined PDMAEMA stars with high arm numbers (up to 24) by ATRP using multifunctional initiators. Quaternization transforms these weak polyelectrolytes into well-characterized strong polyelectrolyte stars. Since the amino groups are much more accessible, PDMAEMA has a higher quaternization efficiency than P2VP.[18−21] DMAEMA is easier to handle than the corresponding acrylate (DMAEA), especially under ATRP conditions. This is reflected, e.g., by the fact that only one publication is available for ATRP of the latter monomer[22] while there are many for DMAEMA.[23−29] Although the molecular weights for linear PDMAEA can be adjusted quite well (initiation efficiencies between 0.6 and 0.9), the molecular weight distributions are rather broad (PDI between 1.4 and 2.0). The substitution of the chain-end halogen by the amine groups of monomer and polymer was given as one possible reason.[22] This effect is less dominant for the sterically hindered PDMAEMA chain-end.

In order to achieve high arm numbers, we used our recently developed initiator, based on a (diglycidylamino)propyl-functional silsesquioxane.[30] Compared to the sugar-based initiators this initiator leads to a higher number of initiation sites per molecule (number-average ca. 58) but exhibits only a small size (diameter around 3 nm). The drawback of this initiator is its finite polydispersity (PDI $\approx$ 1.2) which is due to a mixture of different cage sizes of the silsequioxane core. To the best of our knowledge this is the first report of a hybrid star polyelectrolyte system having a high number of arms. Previous work was related to the synthesis of stars with eight arms employing a regular octahedral silsesquioxane core.[31−34] The goal of the present work is a comprehensive characterization of these systems in dilute aqueous solution by osmometry and dynamic light scattering and a comparison of these results to the predictions of theory.

In subsequent publications we will report on the interaction of these stars with multivalent counterions[35] and their LCST behavior.[36]

Experimental Section

Materials. Anisole, ethyl-α-bromoisobutyrate, *N*,*N*,*N*′,*N*″,*N*‴,*N*‴-hexamethyltriethylenetetraamine (HMTETA), copper bromide (CuBr, $CuBr_2$), methyl iodide, 1,4-dioxane, *trans*-3-indolacrylic acid (IAA), and trimethylsilyldiazomethane were purchased from Aldrich, whereas tetrahydrofuran (THF) and hydrochloric acid (HCl) were delivered from Riedel-de Haën. Acetone, sodium hydroxide (NaOH) and hydrofluoric acid (HF) were bought from Merck. All chemicals were purchased in *pro analysi* (p.a.) quality. Deuterated chloroform ($CDCl_3$) and heavy water (D_2O) were delivered from Deutero, Kastellaun, Germany. These chemicals were used as delivered (except CuBr, which was treated with pure acetic acid and filtered to remove traces of Cu(II) compounds). *N*,*N*-Dimethylaminoethyl methacrylate was donated by RohMax, Darmstadt, and filtered over an alumina B-column before use. The synthesis of the initiators with 5, 8, 21, and 58 initiation sites is described in our previous publications.[7,30] For dialysis we used regenerated cellulose membranes (either ZelluTrans with MWCO 4000−6000 Da from Roth, Karlsruhe, or Spectra/Pore 7 with MWCO 1000 Da).

Synthesis of Star-Shaped Poly(*N*,*N*-dimethylaminoethyl methacrylate). In a typical reaction the monomer *N*,*N*-dimethylaminoethyl methacrylate (45.7 g, 290 mmol), the solvent anisole (150 g), copper(I) bromide (CuBr, 143 mg, 1.0 mmol) and copper(II) bromide ($CuBr_2$, 45 mg, 0.2 mmol) were deoxygenated by purging with nitrogen for 15 min. The solution was heated, under stirring, to 60 °C, yielding a clear, brownish solution. The ligand *N*,*N*,*N*′,*N*″,*N*‴,*N*‴-hexamethyltriethylenetetraamine (270 mg, 1.2 mmol) and the initiator (e.g., 235 mg silsesquioxane-based initiator,[30] 1.16 mmol initiation sites) were dissolved in 5 mL of anisole and purged with nitrogen (15 min). The transfer of the initiator solution to the reaction vessel was performed with a syringe, ensuring as little as possible contact with air. When injecting the initiator/ligand solution, the polymerization mixture immediately turns green. At the appropriate time intervals, samples were drawn with the help of syringes and the conversion was monitored by ^{1}H NMR spectroscopy, comparing the integrals over the signals of the monomeric, unsaturated methylene group (close to 5.6 and 6.2 ppm) with the integrals over the polymeric, methacrylic α-methyl protons (0.6−1.3 ppm). Two polymers with different arm lengths were obtained from each batch by withdrawing a part of the reaction solution at a desired conversion. This was performed with help of a syringe under nitrogen counterflow. For example sample 58A (100 mL of polymerization mixture) was drawn after 675 min at 21% conversion for the polymerization using the silsesquioxane-based initiator. For the workup, the viscous mixtures were diluted with ~200 mL of THF (or acetone) and then passed through a silica column. Hereby copper salt traces were retained. After reconcentration on the rotational evaporator, the polymer was dropwise precipitated into 2 L of cyclohexane/hexane mixtures (volume ratio was 1:2 for polymer 58A). The precipitated polymer was dissolved in dioxane (4 wt %; 100 g dioxane), dialyzed against dioxane for 2 days (Roth membrane, regenerated cellulose, MWCO 4000−6000 Da) and finally freeze-dried from this dioxane solution in the absence of light (to yield, e.g., 4 g of polymer 58A). Direct light exposure and air contact were omitted by storage under nitrogen and below 4 °C. The experimental conditions are given in Table 1. The notations of the polymers are given in the same table together with the expected, theoretical arm length.

Table 1. Experimental Conditions for the Synthesis of Poly(dimethylaminoethyl methacrylate) (PDMAEMA) Stars[a]

run no.[b]	$[DMAEMA]_0$ (mol/L)	t (min)	conversion, x_p[c]	calcd arm length[d]
5A	1.4	175	0.25	63
5E	1.4	485	0.47	118
8A	1.4	175	0.29	73
8E	1.4	485	0.47	118
21A	1.4	420	0.30	75
21E	1.4	1455	0.50	125
58A	1.3	675	0.21	53
58E	1.3	2820	0.41	100

[a] T = 60 °C, $[DMAEMA]_0/[HMTETA]/[Inisite]_0/[CuBr]/[CuBr_2]$ = 250:1:1:0.8:0.2. [b] The number denotes the targeted number of arms; A and E denote short and long arms, respectively. [c] Measured by NMR spectroscopy. [d] Assuming that all initiator functions have initiated.

Synthesis of Star-Shaped Poly{[2-(methacryloyloxy)ethyl] trimethylammonium iodide}. For quaternization, PDMAEMA was dissolved in acetone (2 wt %; e.g. 3 g polymer 58A—0.02 mol amino groups—in 150 g). Methyl iodide (here 4 g, 0.03 mol) was added at room temperature at a molar ratio of 1.5 compared to amino groups. Although the solution became turbid after 10 min the mixture was kept stirring overnight to ensure quantitative conversion. Acetone was decanted and the polymer was washed several times with acetone (each 20 mL). Then 5 g of quaternized polymer was dissolved in 100 mL of water and dialyzed against pure water for 2 days (Roth membrane, regenerated cellulose, MWCO 4000−6000 Da) and finally freeze-dried.

Polymer Characterization. ^{1}H NMR Spectroscopy. A Bruker Avance (250 MHz) spectrometer was used. The solvent was either D_2O or $CDCl_3$. Simulations were performed with ACD/HNMR and ACD/CNMR Predictor Ver.3.00.

Gel Permeation Chromatography (GPC). Apparent molecular weight distributions and their averages of PDMAEMA stars were characterized by GPC using THF with 0.25 wt % tetrabutylammonium bromide (TBAB) as eluent at a flow rate of 0.5 mL/min

Scheme 1. Strategy for the Synthesis of Poly(dimethylaminoethyl methacrylate) (PDMAEMA) Stars with Initiator Example

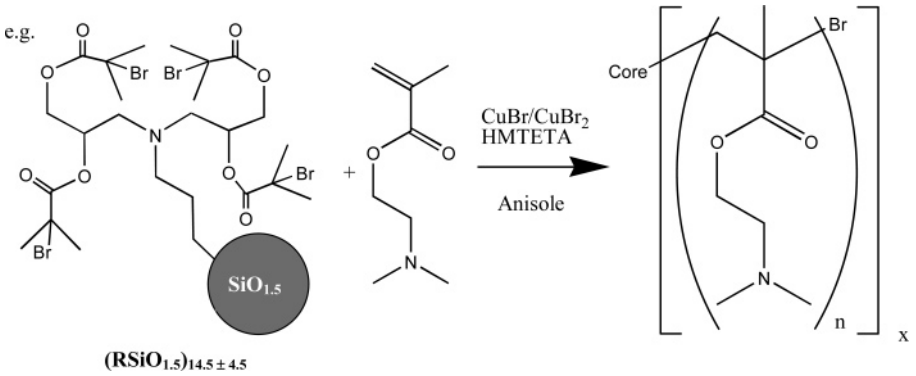

at room temperature (calibration with polystyrene standards). The setup was equipped with four columns (length 30 cm, diameter 0.8 cm, 5 μm PL-Gel, pore sizes 100, 10^3, 10^4, 10^5 Å) and an RI detector.

Asymmetric flow field-flow fractionation (AF−FFF) for the determination of the molecular weight distribution of the quaternized PDMAEMA was accomplished on a Postnova HRFFF-10000 system equipped with RI and multiangle light scattering (Wyatt EOS, $\lambda = 682$ nm) detectors: dimension of the channel, 0.35 mm; cutoff molecular weight of the membrane, 5 kDa; injection volume, 100 μL; constant cross-flow gradient, 1.5 mL/min within 30 min; laminar flow out, 0.6 mL/min; eluent, water with 25 mM sodium nitrate $NaNO_3$ and 0.2 g/L sodium azide NaN_3; sample concentration, 0.7 g/L. For determination of the refractive index increment, one sample (5 mL of a 1.76 g/L solution of quaternized star 58A in eluent) was dialyzed against 150 mL of eluent for 2 days (with help of micro dialyzer QuixSep, Roth, Germany, and Spectra/Por 7 membrane, MWCO 1000) and then diluted with dialysate to obtain different concentrations. The refractive index increment for that sample was determined as $dn/dc = 0.1089 \pm 0.0003$ mL/g on a WGE Dr. Bures DnDc-2010 ($\lambda = 620$ nm) refractometer at room temperature.

Static light scattering (SLS) was performed on a Wyatt EOS ($\lambda = 682$ nm) multiangle light scattering detector, operated in batch mode with acetone as solvent at room temperature (some SLS measurements were performed on a Sofica goniometer using a He−Ne laser). The high sensitivity of the detector enabled us to use very dilute concentrations (in the range 10^{-2} to 10^{-1} g/L). The data were evaluated with the Wyatt ASTRA software, version 4.73.04. All samples were filtered before injection (PTFE filter, 0.45 μm). The refractive index increment was measured with differential refractometer DnDc-2010 (WGE Dr. Bures, $\lambda = 620$ nm) and Differential refractometer Software Ver. 3.24 (Brookhaven Instruments). For samples 21A to 58E the refractive index increment in acetone was determined as $dn/dc = 0.133 \pm 0.02$ mL/g (no change of dn/dc was observed for those high molecular weight stars within the experimental error). For samples 5A to 8E, dn/dc was measured as 0.139 ± 0.04 mL/g.

Dynamic Light Scattering (DLS). For the determination of hydrodynamic radius DLS was performed on an ALV DLS/SLS CGS-8FW compact goniometer system with an ALV 5000/E correlator and a He−Ne laser ($\lambda = 632.8$ nm). Prior to the light scattering measurements (correlation times approximately 300 s depending on signal strength) the sample solutions were filtered using Millipore Nylon filters with a pore size of 0.45 μm. The measured intensity correlation functions were subjected to CONTIN analysis. Apparent hydrodynamic radii of star-shaped polymers were calculated according to the Stokes−Einstein equation, using the viscosity of water. The viscosities of NaCl solutions ($c \geq 0.2$ M) were determined with an Ubbelohde viscometer (Schott, 53610 I), taking the increased densities into account.

Cryogenic Transmission Electron Microscopy (cryo-TEM). The sample was prepared by dissolving 10 mg of quaternized PDMAEMA in 0.5 mL of 1 M NaCl and inserting it into a stiff dialysis cell (micro dialyzer QuixSep) in order to keep the concentration of polymer constant. Dialysis took 2 days against pure water. A drop of the sample was put on an untreated bare copper TEM grid (600 mesh, Science Services, München, Germany), where most of the liquid was removed with blotting paper, leaving a thin film stretched over the grid holes. The specimens were instantly shock-vitrified by rapid immersion into liquid ethane and cooled to approximately 90 K by liquid nitrogen in a temperature-controlled freezing unit (Zeiss Cryobox, Zeiss NTS GmbH, Oberkochen, Germany). The temperature was monitored and kept constant in the chamber during all the sample preparation steps. After freezing the specimens, the remaining ethane was removed using blotting paper. The specimen was inserted into a cryo-transfer holder (CT3500, Gatan, München, Germany) and transferred to a Zeiss EM922 EF-TEM. Examinations were carried out at temperatures around 90 K at an acceleration voltage of 200 kV. Zero-loss filtered images ($\Delta E = 0$ eV) were taken under reduced dose conditions (100−1000 electrons/nm^2). All images were registered digitally by a bottom-mounted CCD camera system (Ultrascan 1000, Gatan) combined and processed with a digital imaging processing system (Gatan Digital Micrograph 3.9 for GMS 1.4).

Osmometry. A membrane osmometer (Gonotec Osmomat 090) with regenerated cellulose membrane (Millipore, PLAC 076 10, NMWL = 1000) was used for the determination of the osmotic coefficient. Solutions of PMETAI (10 g/L) were dialyzed against pure water and diluted to obtain the samples. Solid content determination by freeze drying and vacuum oven (40 °C) gave the final concentration after dialysis. The cell was kept at 30 °C. To rinse the measurement cell with the new sample approximately 0.7 mL of sample solution were injected three times. The measured osmotic pressure Π_m was converted to the osmotic coefficient ϕ, which is defined by the ratio Π_m to the ideal osmotic pressure Π_{cal} of all counterions according to van't Hoff's law (eq 1).[2,5,7]

$$\phi = \frac{\Pi_m}{\Pi_{cal}} \tag{1}$$

For the determination of the number-average molecular weight in THF we used a regenerated cellulose two-layer membrane with MWCO 20000 (Gonotec). Several concentrations were injected and Π_m/c was extrapolated to vanishing concentrations.

Elemental analysis was performed by the Mikroanalytisches Laboratorium Ilse Beetz in Kronach, Germany.

Results and Discussion

Synthesis of Star-Shaped Poly(*N*,*N*-dimethylaminoethyl methacrylate). We performed the synthesis of star-shaped PDMAEMA by atom transfer radical polymerization employing oligofunctional initiators with 2-bromoisobutyryl initiating fragments, with copper bromide CuBr as catalyst and *N*,*N*,*N*′,*N*″,*N*‴,-*N*‴-hexamethyltriethylenetetramine as a strong ligand in anisole as solvent (Scheme 1).[24] To minimize the concentration of free

Table 2. Molecular Weight Averages (in g/mol) of Poly(dimethylaminoethyl methacrylate) Stars Determined by Different Methods

sample	$10^{-3}M_{n,calc}$[a]	$10^{-3}M_{n,exp}$[b]	$10^{-3}M_{n,app}$[c] (PDI_{app})	$10^{-3}M_w$[d] ($\langle R^2_g\rangle_z^{0.5}$ [nm])	PDI[e]
5A	51	56	42 (1.13)	62 (-)	1.22
5E	94	97	74 (1.21)	103 (-)	1.10
8A	93	99	67 (1.09)	117 (-)	1.26
8E	150	155	108 (1.14)	155 (-)	1.03
21A	250		162 (1.11)	300 (-)	1.20
21E	430		248 (1.18)	560 (23)	1.30
58A	490	500	253 (1.12)	690 (17)	1.41
58E	950	950	371 (1.24)	1360 (29)	1.43

[a] Number-average molecular weight (M_n) calculated from conversion $x_{p,NMR}$ ($M_n = M_{DMAEMA} \times x_{p,NMR} \times [DMAEMA]_0$ /[initiator molecule]$_0$). [b] Experimental M_n determined by membrane osmometry in THF for 5A to 8E and by elemental analysis for 58A/58E. [c] Apparent M_n determined by gel permeation chromatography with linear poly(styrene) standards. [d] Weight-average molecular weight (M_w) and root of *z*-average of mean-squared radius of gyration (R_g) determined by static light scattering (SLS) in acetone. [e] Polydispersity index (*PDI*) determined by ratio of M_w (SLS) and M_n (conversion).

radicals and hence reduce termination we added $CuBr_2$ as a retarder.

In addition to initiators based on glucose (five functions), saccharose (eight functions), or β-cyclodextrin (21 functions),[7] we employed a silsesquioxane-based initiator with ca. 58 functions, which has already been used for the synthesis of star-shaped glycopolymers and hybrid poly(acrylic acid) stars with inorganic core (Scheme 1).[30]

The kinetics of those polymerizations depends on the number of initiating sites. Details are reported in the Supporting Information. By withdrawing samples at different conversions we obtained a range of polymers with different arm numbers and arm lengths. The notation is shown in Table 1. From ratio of monomer to initiating site concentrations and conversion we calculated the theoretical arm lengths by assuming that initiation site efficiency equals unity (see Table 1). Since the monomer is quite bulky, the initiation site efficiency was expected to be below unity, leading to less, but longer arms. However, the overall number-average molecular weight, M_n, does not change (see Table 2), given that each initiator molecule initiates at least once and chain transfer and chain−chain coupling can be excluded.

Molecular Characterization. We performed gel permeation chromatography (GPC) in THF with 0.25 wt % tetrabutylammonium bromide (TBAB) to minimize the adsorption of the amino-containing polymer on the column. Typical eluograms are given in Figure 1. The apparent molecular weight averages and polydispersity indexes (calibration with linear polystyrene) are given in Table 2.

In Figure 1 we observe the expected increase of the hydrodynamic volume with increasing arm length as well with increasing arm number. In the case of the sugar-based stars a small fraction of star−star coupling is observed as a small shoulder on the low elution volume side of the eluogram. In contrast, almost no shoulder is found for the PDMAEMA stars with high arm numbers. This might be due to the decreased radical concentration in the synthesis of silsesquioxane-based stars (lower polymerization rate, see Supporting Information). The polydispersity of the silsesquioxane initiator might also obscure the visibility of coupled products. The apparent polydispersity of the stars, which mainly resembles the polydispersity in hydrodynamic radius, increases with conversion in all cases (see Table 2). This might reflect some termination reactions like disproportionation or star−star coupling reactions by either combination of chain end radicals or the attack of amines on the chain end halogen (see also Supporting Information). Both effects should be the more pronounced the better the stars can interpenetrate.

The absolute number-average molecular weight, M_n, of the stars with lower arm numbers was determined by membrane osmometry in THF (Table 2). For the stars with silsesquioxane core the determination of M_n was performed by elemental analysis, comparing the silicon and bromine contents, which originated from the initiator, with the nitrogen content of the monomer units (see Table S-1, Supporting Information). The obtained values are close to the expected values, which we calculated from conversion. This means that conversions determination by NMR, osmometry and elemental analysis are reliable methods for the determination of M_n of those PDMAEMA stars.

To determine the real polydispersity of the stars, we performed static light scattering experiments in very dilute acetone solutions of PDMAEMA on a multiangle light scattering detector. One example of an obtained Zimm plot is given in Figure 2. All results are listed in Table 2. The polydispersity index is calculated as the ratio of M_w, determined by SLS, to M_n, determined by conversion. Since both values have inherent errors, the error in the PDI is larger than that obtained by GPC, but it is not as systematic. GPC of multiarm stars suffers from the problem that the hydrodynamic volume does not depend as strongly on the arm number as on the arm length.[37]

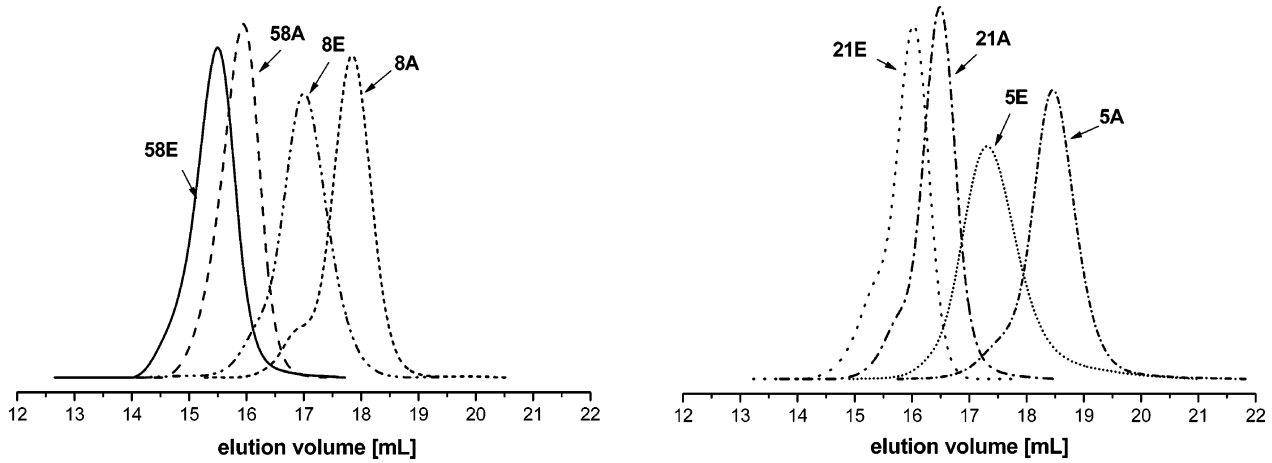

Figure 1. Gel permeation chromatography eluograms of poly(dimethylaminoethyl methacrylate) stars with tetrahydrofuran (+0.25 wt % tetrabutylammonium bromide) as eluent.

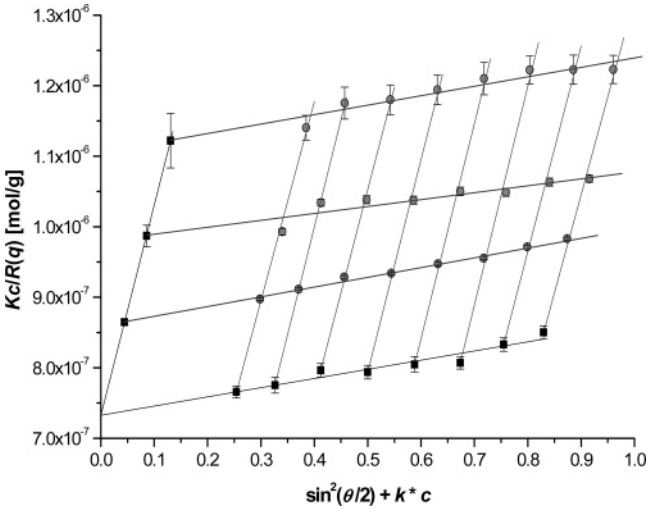

Figure 2. Zimm plot of poly(dimethylaminoethyl methacrylate) star 58E in acetone at 25 °C (k = 2 L/g; concentration c = 0.022, 0.043, and 0.066 g/L).

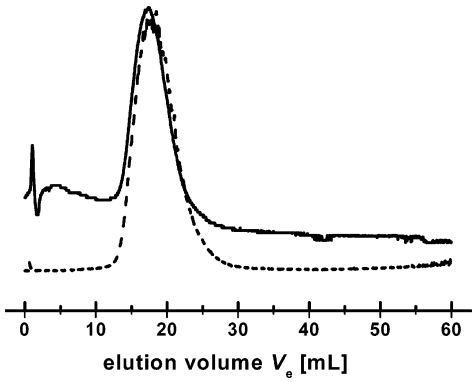

Figure 3. Field-Flow Fractionation (AF−FFF) eluogram of quaternized star 58 A in water (0.7 g/L; 25 mM $NaNO_3$, 0.2 g/L NaN_3; solid line, RI detector; dashed line, multiangle light scattering (MALS) detector at 90°).

As seen in Table 2 silsesquioxane-based stars have higher polydispersity than the sugar-based stars. One should keep in mind that the initiator is polydisperse (PDI = 1.2). The increase in polydispersity as compared to the initiators indicates an additional arm number distribution due slow initiation.[38] Polydispersity due to arm-length variation is rather negligible, as implied by Schulz's coupling theorem.[39] Though the apparent polydispersity by GPC increases during polymerization in all cases it is striking that the polydispersities appear to decrease with conversion for the stars with low arm numbers.

Quaternization of PDMAEMA Stars. In order to obtain strong polyelectrolyte stars, the pendant amino groups were quaternized with methyl iodide, leading to poly{[2-(methacryloyloxy)ethyl] trimethylammonium iodide} (PMETAI). The completeness of quaternization was verified by elemental analysis, ^{1}H NMR (Figure S-2, Supporting Information) and by asymmetric flow field-flow fractionation (AF−FFF) with multiangle light scattering detector (Figure 3).

The distribution stays monomodal after quaternization. The obtained weight-average molecular weight, M_w, from the multiangle light scattering detector is 1.5×10^6 g/mol which is consistent with the expected M_w of 1.3×10^6 g/mol. The polydispersity obtained by AF-FFF-MALS is underestimated (PDI = 1.1) which might be a result of the poor separation of starlike molecules with an arm-number distribution. The change in molecular weight is only weakly reproduced in a change of hydrodynamic volume as also seen in GPC, where we obtained almost the same apparent polydispersity.

Determination of Initiation Site Efficiency. The arms of the quaternized PDMAEMA were detached from the core by classical ester hydrolysis in concentrated NaOH. The resulting linear PMAA was analyzed by aqueous GPC and additionally esterified to PMMA, which was analyzed by GPC and MALDI−ToF mass spectrometry. The details of procedure and analysis are given in the Supporting Information and the results are listed in Table 3.

In addition to the classical method one can estimate the initiation site efficiency of the silsesquioxane-based stars by cleaving off segments with four former initiation sites. These are linked via silicon atoms to the silsesquioxane core and can be released by treatment with hydrofluoric acid (Scheme 2).

^{1}H NMR does not give any indication of ester cleavage as the integrals over the signals are the same before and after HF treatment and dialysis, whereas GPC (in THF with TBAB) reveals 100% scission (Figure 4). Although one would expect a quadrimodal distribution, showing fragments with one, two, three and four arms, the limited GPC resolution only provided a bimodal distribution. Thus, we performed a double Gaussian fit in the distinct region of the eluogram. Furthermore, the tailing indicates that the low molecular fraction (including the low

Table 3. Number-Average Degrees of Polymerization of the Cleaved Arms and Their Polydispersities (in Parentheses, Both Obtained by Different Methods), Initiation Site Efficiencies, f_i, Derived Therefrom (*Bold Italics*) and the Approximate Formulas Derived from the Averages of Initiation Site Efficiencies

method	5A	5E	8A	8E
conversion[a]	63; ***1.00***	118; ***1.00***	73; ***1.00***	118; ***1.00***
GPC of lin. PMAA[b]	101 (1.37); ***0.62***	169 (1.32); ***0.70***	113 (1.40); ***0.65***	169 (1.34); ***0.70***
GPC of lin. PMMA[c]	102 (1.09); ***0.62***	162 (1.13); ***0.73***	116 (1.09); ***0.63***	167 (1.12); ***0.71***
MALDI of PMMA[d]	104 (1.15); ***0.61***	154 (1.15); ***0.77***	99 (1.17); ***0.73***	171 (1.13); ***0.69***
av	***0.62***	***0.73***	***0.67***	***0.70***
formula[e]	$(PDMAEMA_{100})_{3.1}$	$(PDMAEMA_{160})_{3.7}$	$(PDMAEMA_{110})_{5.4}$	$(PDMAEMA_{170})_{5.6}$
method	21A	21E	58A	58E
conversion[a]	75; ***1.00***	125; ***1.00***	53; ***1.00***	100; ***1.00***
GPC of lin. PMAA[b]	173 (1.32); ***0.43***	264 (1.33); ***0.47***	173 (1.38); ***0.31***	238 (1.45); ***0.42***
GPC of lin. PMMA[c]	147 (1.16); ***0.51***	223 (1.31); ***0.56***	161 (1.21); ***0.33***	242 (1.31); ***0.41***
MALDI of PMMA[d]	177 (1.07); ***0.42***	(385 (1.06); ***0.32***)	188 (1.08); ***0.28***	233 (1.05); ***0.43***
average	***0.45***	***0.51***	***0.31***	***0.42***
formula[e]	$(PDMAEMA_{170})_{9.5}$	$(PDMAEMA_{240})_{11}$	$(PDMAEMA_{170})_{18}$	$(PDMAEMA_{240})_{24}$

[a] Expected degree of polymerization P_n obtained by conversion $x_{p,NMR}$ and monomer to initiator ratio ($P_n = x_{p,NMR}[DMAEMA]_0$ /[initiator molecule]$_0$). [b] P_n obtained by gel permeation chromatography (GPC) of corresponding poly(methacrylic acid) (PMAA) with water as eluent. [c] GPC of corresponding poly(methyl methacrylate) (PMMA) with tetrahydrofuran as eluent. [d] Obtained by matrix assisted laser desorption ionization time-of-flight (MALDI-ToF) mass spectrometry of corresponding PMMA arms. [e] Structure of poly(dimethylaminoethyl methacrylate) stars $(PDMAEMA_n)_x$; n = number-average degree of polymerization per arm; x = number-average arm number.

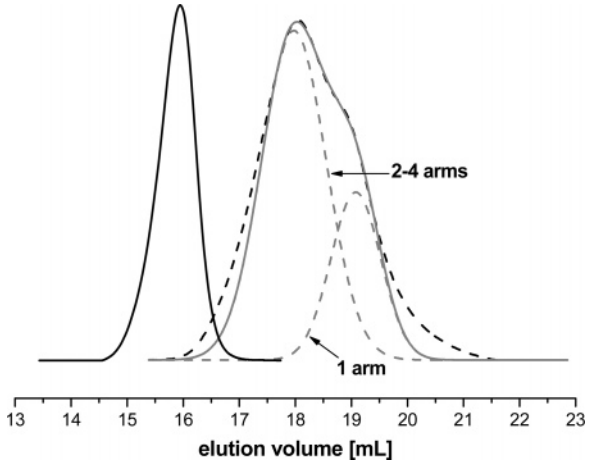

Figure 4. Gel permeation chromatography eluograms of poly(dimethylaminoethyl methacrylate) (PDMAEMA) star 58A (−) and its single fragments, obtained by HF treatment of core (− −), and (in gray) the deconvolution of the PDMAEMA star fragments by a double Gaussian fit (−) with its single constituents (− −).

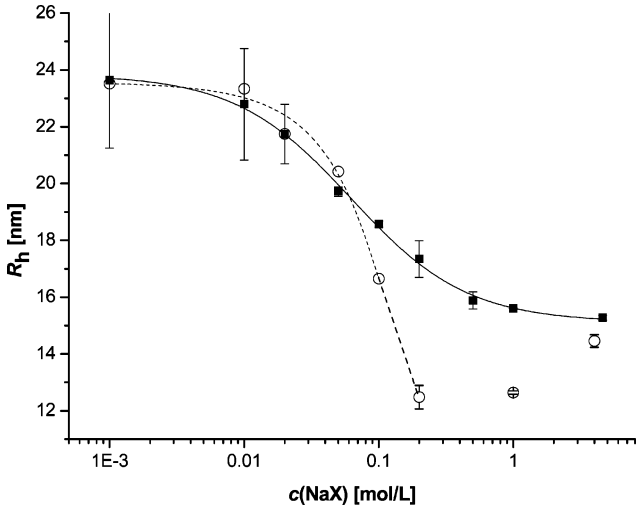

Figure 5. Dependence of the hydrodynamic radius of star-shaped quaternized poly(dimethylaminoethyl methacrylate) 58A, $(PMETAI_{170})_{18}$, with ionic strength; squares: NaCl; circles: NaI. The lines are guides for the eye.

molecular residual) is linear PDMAEMA with only one arm, as the tailing strongly resembles the trace of linear PMMA (former PDMAEMA arms; not shown). The high molecular weight fraction comprises all segments with higher arm numbers. Assuming Bernoullian statistics, which implies independent occurrence of single initiation processes, we can now make a further rough estimation of the initiation site efficiency. In order to compare the expected probability of having segments with x arms with the response of the mass-sensitive RI-detector one needs to multiply the probability with x. By trial and error

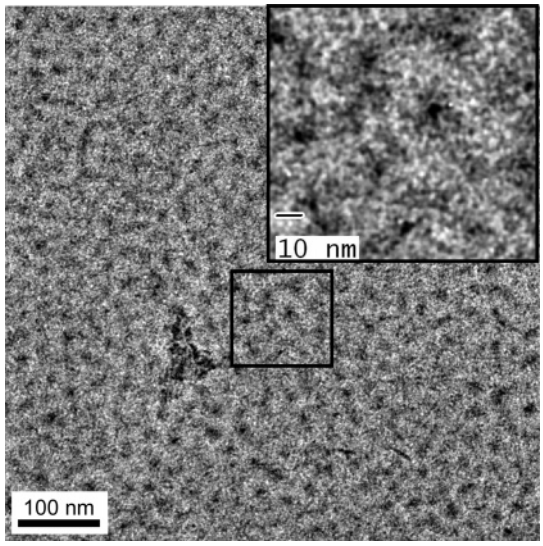

Figure 6. Cryogenic transmission electron microscopy (cryo-TEM) image of a 2 wt % solution of quaternized poly(dimethylaminoethyl methacrylate) 58A, $(PMETAI_{170})_{18}$, in water (the iodide counterion was partly exchanged by chloride during dialysis). Inset: zoom of the marked region.

Table 4. Bernoullian Probabilities of Finding Detached Stars with x Arms out of Maximum Four

x	probability calculation	mole fraction $n(x)$ for $p = 0.33$	weight fraction $w(x) = x \cdot n(x)$
0	$(1-p)^4$	0.202	0
1	$(1-p)^3 \times p \cdot 4$	0.397	0.300
2	$(1-p)^2 \times p^2 \times 6$	0.293	0.444 }
3	$(1-p) \times p^3 \times 4$	0.096	0.219 } $\Sigma = 0.70$
4	p^4	0.012	0.036 }

we estimated the initiation site efficiency to be $p = 0.33$ (Table 4), which coincides nicely with the initiation site efficiency obtained by classical cleavage, $f_i = 0.31$. This value fits best the ratio of RI response integrals A in GPC, A(2−4 arms)/A(one arm) = 0.7/0.3 = 2.3.

The same procedure was attempted for 58 E. However as the initiator has a higher initiation site efficiency in that case, the ratio of fragments with only one arm is rather small and, due to GPC's limited resolution for fragments with higher arm number and longer arms, fitting was not feasible. Besides the limited resolution of the GPC, the same hydrodynamic volume can be expected for segments with many short arms and segments with a few long arms. Because of slow initiation both types of segments might be present in our sample and aggravate the analysis since both types of segments overlap in the GPC eluogram.

Another drawback of the new method is the assumption of purely independent initiation processes. We cannot exclude that after one initiation site has initiated, the probability to initiate

Scheme 2. Destruction of the Core of Silsesquioxane-Based Stars (R Assigns F or OH)

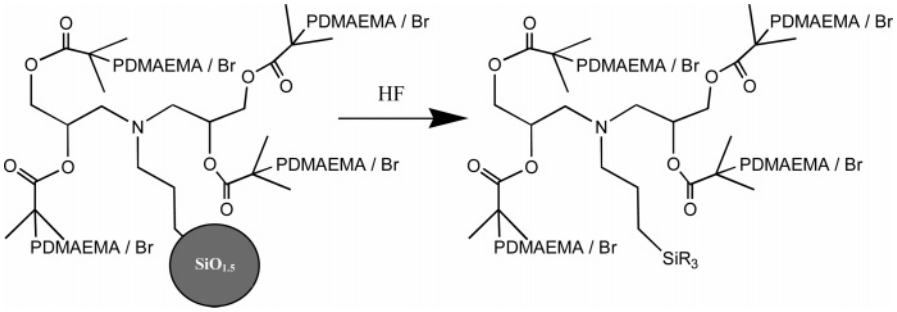

Table 5. Dynamic Light Scattering (DLS) Results of the Poly(dimethylaminoethyl methacrylate) Stars in Acetone[a] and the Structure-Sensitive Parameter, ρ, Calculated Using the Radius of Gyration $\langle R_g^2\rangle_z^{0.5}$ from Table 2

	5A $(PDMAEMA_{100})_{3.1}$	5E $(PDMAEMA_{160})_{3.7}$	8A $(PDMAEMA_{110})_{5.4}$	8E $(PDMAEMA_{170})_{5.6}$
$\langle R_h\rangle_z$ [nm][b]	4.7	6.1	6.0	7.4
$\langle R_h\rangle_w/\langle R_h\rangle_n$[c]	1.22	1.36	1.12	1.20
	21A $(PDMAEMA_{170})_{9.5}$	21E $(PDMAEMA_{240})_{11}$	58A $(PDMAEMA_{170})_{18}$	58E $(PDMAEMA_{240})_{24}$
$\langle R_h\rangle_z$ [nm][b]	8.7	14.7	13.5	19.9
$\langle R_h\rangle_w/\langle R_h\rangle_n$ c	1.08	1.20	1.13	1.31
$\rho = \langle R_h\rangle_z/\langle R_g^2\rangle_z^{0.5}$	-	1.5	1.3	1.5

[a] Concentration 0.4 g/L at 25 °C, except 21E, 58A and 58E: 0.2 g/L. [b] *z*-average hydrodynamic radius R_h obtained by CONTIN analysis. [c] Polydispersity in hydrodynamic radius obtained by weight- and number-average hydrodynamic radius according to CONTIN analysis.

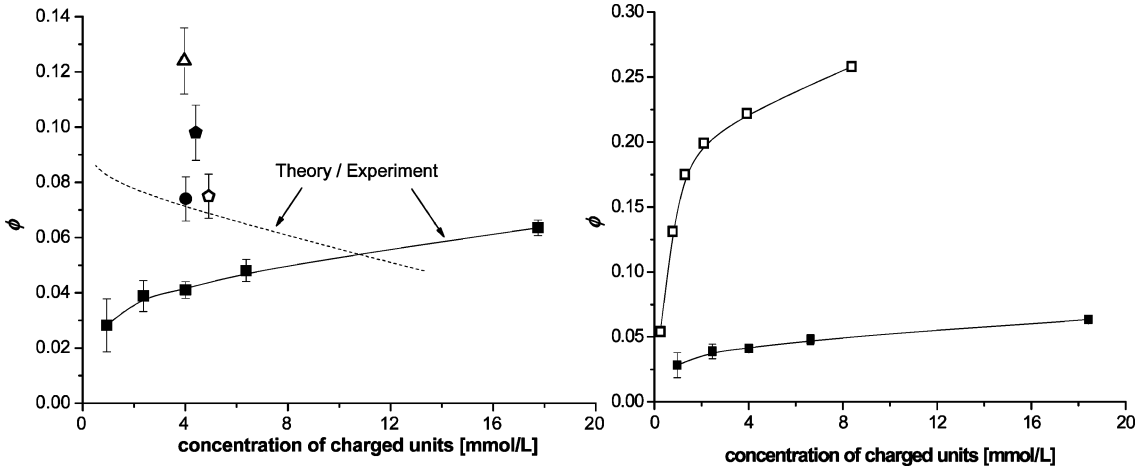

Figure 7. Osmotic coefficients, Φ, of star-shaped poly{[2-(methacryloyloxy)ethyl] trimethylammonium iodide} $(PMETAI_{170})_{18}$ (58A, ■), $(PMETAI_{170})_{9.5}$ (21A, ●), $(PMETAI_{110})_{5.4}$ (8A, ⬠), $(PMETAI_{170})_{5.6}$ (8E, ⬟), and $(PMETAI_{100})_{3.1}$ (5A, △). Dashed line: theoretical dependence for a fully ionized star with 18 arms and degree of polymerization of single arm $DP_{arm} = 170$. Right-hand side: comparison of $(PMETAI_{170})_{18}$ with poly(acrylic acid) star $(PAA_{100})_{21}$ with degree of neutralization, $\alpha = 0.24$.[7]

the surrounding initiation sites has decreased due to decreased accessibility. This is not taken into account by Bernoullian statistics.

Hydrodynamic Behavior. We performed dynamic light scattering (DLS) measurements on the uncharged PDMAEMA stars in acetone at concentrations below the overlap concentration (0.4 g/L at 25 °C except for 21E, 58A, and 58E, which are 0.2 g/L) and on the quaternized stars (PMETAI) in aqueous salt solutions. The intensity autocorrelation function of star-shaped PDMAEMA was determined for different scattering angles. A linear dependence of the decay rates, Γ, on the squared length of scattering vector, q^2, was found in all cases, indicating a purely diffusive process of spherical star polymers.

The hydrodynamic radii of some PDMEMA stars, obtained by CONTIN analysis at 90°, are summarized in Table 5. The polydispersity, as seen from this analysis, increases with the arm length (i.e increasing conversion). This coincides with the apparent polydispersities seen in conventional GPC (Table 2) which reflect the distribution of hydrodynamic volumes.

The observed structure-sensitive parameters, $\rho = \langle R_h\rangle_z/\langle R_g^2\rangle_z^{0.5}$, are typical for starlike structures. Burchard's derivation[40] leads to $\rho = 1.30$ and 1.37 for stars with 24 and 11 polydisperse arms, respectively, under Θ-conditions. Since our measurements were performed in a good solvent, these theoretical ratios should increase, matching our experimental parameters.

The dependence of the hydrodynamic radius, R_h, of the star-shaped quaternized PDMAEMA 58A, $(PMETAI_{170})_{18}$, on ionic strength was also investigated by DLS ($c = 0.3$ g/L, 24 °C, 90°). For very low salt concentrations the intensity-weighted decay rate distributions (after CONTIN treatment of the intensity autocorrelation curves) tend to broaden, most probably due to increasing inter-particle interactions, e.g., slow modes.

For the determination of the hydrodynamic radii, according to the Stokes−Einstein equation, the viscosities of NaCl and NaI solutions were measured and taken into account. At low ionic strength ($c_{NaX} < 0.01$ M) we found $R_h \sim 24$ nm, which is about 56% of the contour length of a single chain ($L_c = 0.25$ nm × $DP_{n,arm} = 42.5$ nm), indicating a considerable stretching due to Coulombic repulsion and high osmotic pressure inside the star. Figure 5 shows a pronounced drop in hydrodynamic radius with increasing salt concentration, indicating the expected contraction of the polyelectrolyte arms due to electrostatic and osmotic screening (diminishing the high net osmotic pressure within the star). The hydrodynamic radius in the fully salted case ($R_h \sim 15$ nm at 4.6 M NaCl) is in good agreement with that of the uncharged PDMAEMA star 58A in acetone ($R_h \sim 14$ nm).

Figure 5 also demonstrates that these cationic star polyelectrolytes exhibit a salting-out and a salting-in effect as observed previously for cationic spherical[41] and planar brushes.[42] Using NaI instead of NaCl leads to the same hydrodynamic radius at low salt concentration but to marked differences starting from $c \sim 0.1$ M. At 0.5 M NaI the system enters a two-phase region but at 1 M NaI a salting-in occurs. This collapse transition in a single starlike molecule is under further investigation.

Cryogenic Transmission Electron Microscopy. Finally we characterized the quaternized PDMAEMA star 58A, $(PMETAI_{170})_{18}$, by cryo-TEM. The star polymer was dissolved in 1 M NaCl and dialyzed against pure water which leads to a

partial exchange of iodide ions. Distinct structures are seen in Figure 6. In some cases the silsesquioxane cores are apparent as dark spots with a diameter in the range of 3 nm (insert). According to Fourier transformation the mean distance between the particle centers is around 27 nm, i.e., above the overlap concentration (hydrodynamic diameter, $2R_h \approx 48$ nm). Still we observe some fading shades around the core, which might be attributed to the radially decreasing segment density. Because of the slow initiation during polymerization the segment density around the core is higher than in the case of uniform arms.

Osmotic Coefficients. Recently we published the osmotic behavior of star-shaped poly(acrylic acid) (PAA) with rather low degree of neutralization.[7] Here we present the osmotic coefficient of fully charged, quaternized PDMAEMA stars.

Figure 7 shows that the osmotic coefficients decrease with increasing arm number and decreasing arm length. In both cases the segment density and thus the charge density and thus the counterion confinement increase.[3]

Figure 7 (right-hand side) compares $(PAA_{100})_{21}$ and $(PMETAI_{170})_{18}$, both having comparable arm numbers and arm lengths but different charge densities. We directly see that increasing charge density leads to larger counterion confinement, as predicted by theory.[3]

For $(PMETAI_{170})_{18}$ (58A), we also investigated the concentration dependence. We see again an increase of the osmotic coefficient with concentration, though the rise is not as large as for the PAA stars. However, the observed concentration dependence is in contrast to theory[3] as was already discussed for the PAA stars.[7] Nevertheless, both theory and experiment give values in the same order of magnitude. Some deviations might arise due to the polydisperse nature of our stars and due to possible ion-specific interactions. The differences between the concentration dependences might also stem from the fact that the theory regards all counterions outside the star to have equal osmotic activity even though the counterions in the close vicinity experience a strong electrostatic field, diminishing their activity. Increasing concentration can give a contribution to a higher activity of those counterions since the decreasing distance between the stars alters the net electrostatic field. In theory, the entropic contribution of the counterions leads to an increased number of free counterions in respect to decreasing concentration. Nevertheless, we can conclude that more than 90% of the counterions are entrapped within the investigated quenched polyelectrolyte star 58A. This is in full agreement with theory.

Conclusions

Star-shaped PDMAEMAs and their quaternized analogues, PMETAI, were successfully synthesized by the core-first method employing ATRP. The architecture of the initiating system together with the polymerization features lead to polymer stars with a moderate arm number and arm size distribution due to slow initiation. The initiation site efficiency was determined by two different cleaving procedures: cleaving off all of the arms and detaching starlike fragments. The obtained star-shaped strong polyelectrolytes show the expected decrease in hydrodynamic radius with increasing ionic strength. For iodide counterions a salting-out/salting-in effect is observed. Up to 97% of counterions are confined inside the star, as determined by osmometry in salt-free solution. The confinement increases with increasing arm number and decreasing arm length. However, again there is a discrepancy between the experimentally observed and theoretically calculated concentration dependence of the osmotic coefficients, which needs further elaboration.

Acknowledgment. This work was supported by the Deutsche Forschungsgemeinschaft within SFB 481 and by the Fonds der Chemischen Industrie. We thank Manuela Schumacher, Cornelia Rettig and Denise Danz for the MALDI−ToF MS measurements, Youyong Xu, Sabine Wunder, Daniela Kropp and Klaus Kreger for GPC measurements, Markus Burkhardt and Markus Ruppel for their help during SLS/DLS measurements and Andrew Ah Toy for proof-reading the manuscript.

Supporting Information Available: Text giving the kinetics of ATRP of DMAEMA with multifunctional initiators including experimental details of arm cleavage and release of starlike segments by treatment with HF and details of elemental analysis of silsesquioxane-based stars, including figures showing kinetic plots, H NMR spectra, molecular weight distributions, and mass spectra, a table giving elemental analysis data, and a scheme showing the chemical modifications used. This material is available free of charge via the Internet at http://pubs.acs.org.

References and Notes

(1) Pincus, P. *Macromolecules* **1991**, *24*, 2912−2919.
(2) Jusufi, A.; Likos, C. N.; Löwen, H. *Phys. Rev. Lett.* **2002**, *88*, 018301.
(3) Jusufi, A.; Likos, C. N.; Löwen, H. *J. Chem. Phy.* **2002**, *116*, 11011−11027.
(4) Das, B.; Guo, X.; Ballauff, M. *Prog. Colloid Polym. Sci.* **2002**, *121*, 34−38.
(5) Deserno, M.; Holm, C.; Blaul, J.; Ballauff, M.; Rehahn, M. *Eur. Phys. J. E* **2001**, *5*, 97−103.
(6) Jusufi, A.; Likos, C. N.; Ballauff, M. *Colloid Polym. Sci.* **2004**, *282*, 910−917.
(7) Plamper, F. A.; Becker, H.; Lanzendörfer, M.; Patel, M.; Wittemann, A.; Ballauff, M.; Müller, A. H. E. *Macromol. Chem. Phys.* **2005**, *206*, 1813−1825.
(8) Zilliox, J. G.; Rempp, P.; Parrod, J. *J. Polym. Sci. Pol Sym.* **1968**, No. *22* (Pt. 1), 145−156.
(9) Luxton, A. R.; Quig, A.; Delvaux, M. J.; Fetters, L. J. *Polymer* **1978**, *19* (11), 1320−1324.
(10) Tsitsilianis, C.; Voulgaris, D. *Macromol. Chem. Phys.* **1997**, *198*, 997−1007.
(11) Simmons, M. R.; Yamasaki, E. N.; Patrickios, C. S. *Polymer* **2000**, *41*, 8523−8529.
(12) Vamvakaki, M.; Patrickios, C. S. *Chem. Mater.* **2002**, *14*, 1630−1638.
(13) Georgiou, T. K.; Vamvakaki, M.; Phylactou, L. A.; Patrickios, C. S. *Biomacromolecules* **2005**, *6*, 2990−2997.
(14) Haddleton, D. M.; Edmonds, R.; Heming, A. M.; Kelly, E. J.; Kukulj, D. *New J. Chem.* **1999**, *23*, 477−479.
(15) Ohno, K.; Wong, B.; Haddleton, D. M. *J. Polym. Sci., Polym. Chem.* **2001**, *39*, 2206−2214.
(16) Hu, H.; Fan, X.; Huang, Y. *Gaofenzi Xuebao* **2004**, *6*, 805−811.
(17) Li, J.; Xiao, H.; Kim, Y. S.; Lowe, T. L. *J. Polym. Sci. Polym. Chem.* **2005**, *43*, 6345−6354.
(18) Strauss, U. P.; Layton, L. H. *J. Phys. Chem.* **1953**, *57*, 352−354.
(19) Frere, Y.; Gramain, P. *Macromolecules* **1992**, *25*, 3184−3189.
(20) Chovino, C.; Gramain, P. *Macromolecules* **1998**, *31*, 7111−7114.
(21) Bicak, N.; Gazi, M. *J. Macromol. Sci. Pure* **2003**, *A40*, 585−591.
(22) Zeng, F.; Shen, Y.; Zhu, S. *Macromol. Rapid Commun.* **2002**, *23*, 1113−1117.
(23) Xia, J.; Johnson, T.; Gaynor, S. G.; Matyjaszewski, K.; DeSimone, J. *Macromolecules* **1999**, *32*, 4802−4805.
(24) Zeng, F.; Shen, Y.; Zhu, S.; Pelton, R. *Macromolecules* **2000**, *33*, 1628−1635.
(25) Fang, Z.; Kennedy, J. P. *J. Polym. Sci. Polym. Chem.* **2002**, *40*, 3679−3691.
(26) Lee Sang, B.; Russell Alan, J.; Matyjaszewski, K. *Biomacromolecules* **2003**, *4*, 1386−1393.
(27) Zheng, G.; Stoever, H. D. H. *Macromolecules* **2003**, *36*, 7439−7445.
(28) Mao, B.; Gan, L.-H.; Gan, Y.-Y.; Li, X.; Ravi, P.; Tam, K.-C. *J. Polym. Sci., Polym. Chem.* **2004**, *42*, 5161−5169.
(29) Lee, H.-i.; Pietrasik, J.; Matyjaszewski, K. *Macromolecules* **2006**, *39*, 3914−3920.
(30) Muthukrishnan, S.; Plamper, F.; Mori, H.; Müller, A. H. E. *Macromolecules* **2005**, *38*, 10631−10642.
(31) Majoros, I.; Marsalko, T. M.; Kennedy, J. P. *Polym. Bull. (Berlin)* **1997**, *38*, 15−22.
(32) Costa, R. O. R.; Vasconcelos, W. L.; Tamaki, R.; Laine, R. M. *Macromolecules* **2001**, *34*, 5398−5407.
(33) Costa, R. O. R.; Vasconcelos, W. L.; Laine, R. M. *Materials Research* (*Sao Carlos, Brazil*) **2002**, *5*, 247−252.

(34) Mengel, C.; Meyer, W. H.; Wegner, G. *Macromol. Chem. Phys.* **2001**, *202*, 1138−1149.
(35) Plamper, F. A.; Walther, A.; Müller, A. H. E.; Ballauff, M. *Nano Lett.* **2007**, *7*, 167−171.
(36) Plamper, F. A.; Ruppel, M.; Schmalz, A.; Borisov, O.; Ballauff, M.; Müller, A. H. E. *Macromolecules* **2007**, submitted for publication.
(37) Daoud, M.; Cotton, J. P. *J. Phys. Paris* **1982**, *43*, 531.
(38) Gold, L. *J. Chem. Phys.* **1958**, *28*, 91−99.
(39) Schulz, G. V. *Z. Phys. Chem.* (*Leipzig*) **1939**, *B43*, 25.
(40) Burchard, W.; Schmidt, M.; Stockmayer, W. H. *Macromolecules* **1980**, *13*, 1265−1272.
(41) Mei, Y.; Ballauff, M. *Eur. Phys. J. E* **2005**, *16*, 341−349.
(42) Biesalski, M.; Johannsmann, D.; Rühe, J. *J. Chem. Phys.* **2004**, *120*, 8807−8814.

MA070452X